Granular packings of elongated faceted particles deposited under gravity

J. Stat. Mech. (2010) P06025

(http://iopscience.iop.org/1742-5468/2010/06/P06025)

Journal of Statistical Mechanics: Theory and Experiment
An IOP and SISSA journal

Granular packings of elongated faceted particles deposited under gravity

Raúl Cruz Hidalgo[1], Iker Zuriguel[2], Diego Maza[2] and Ignacio Pagonabarraga[3]

[1] AMADE, Departament de Física, Av. Montilivi s/n, Universitat de Girona, 17071 Girona, Spain
[2] Departamento de Física y Matemática Aplicada, Facultad de Ciencias, Universidad de Navarra, 31080 Pamplona, Spain
[3] Departament de Física Fonamental, Carrer Martí i Franqués, 1, Universitat de Barcelona, 08028 Barcelona, Spain
E-mail: raul.cruz@udg.edu, iker@fisica.unav.es, dmaza@unav.es and ipagonabarraga@ub.edu

Received 21 January 2010
Accepted 1 June 2010
Published 28 June 2010

Online at stacks.iop.org/JSTAT/2010/P06025
doi:10.1088/1742-5468/2010/06/P06025

Abstract. We report experimental and theoretical results of the effect that particle shape has on the packing properties of granular materials. We have systematically measured the particle angular distribution, the cluster size distribution and the stress profiles of ensembles of faceted elongated particles deposited in a bidimensional box. Stress transmission through this granular system has been numerically simulated using a two-dimensional model of irregular particles. For grains of maximum symmetry (squares), the stress propagation localizes and forms chain-like forces analogous to those observed for granular materials composed of spheres. For thick layers of grains, a pressure saturation is observed for deposit depths beyond a characteristic length. This scenario correlates with packing morphology and can be understood in terms of stochastic models of aggregation and random multiplicative processes. As grains elongate and lose their symmetry, stress propagation is strongly affected. Lateral force transmission becomes less favored than vertical transfer, and hence, an increase in the pressure develops with depth, hindering force saturation.

Keywords: granular matter, jamming and packing

1742-5468/10/P06025+17$30.00

Contents

1. Introduction

Granular materials are of great significance nowadays in engineering and physics [1]–[4]. Huge experimental and theoretical efforts have been made to try and obtain a better understanding of the global behavior of these many-body systems in terms of local particle–particle interactions. In granular packing, forces are generally transferred from particle to particle through contacts and force chains which can branch at a grain and generate a beautiful force network [5]–[9]. Particles outside these force chains support practically no load and can be removed from the packing without changing the global mechanical properties of the system. Additionally, in granular materials the frictional interactions between particles are generally nonlinear and even discontinuous. This makes it very difficult to predict and control their behavior and opens up many conceptual challenges regarding their description [1]–[4].

Despite the fact that granular media, such as rice, lentils or pills, are often composed of grains with anisotropic shapes, most experimental and theoretical studies have concerned spherical particles [1]–[3]. In the last decade many different studies have proved that the introduction of modifications in the particle shape may give rise to completely different physical scenarios [10]–[14]. These include the effect of particle shape on packing fraction [11, 12], wall pressures in a silo discharge [13], coordination number [14], jamming [15], and stress propagation in granular piles [16]. Despite these efforts, the aspect ratio has only very recently been systematically modified to analyze the special features that particle shape asymmetry may introduce in the packing [11], [17]–[19]. Moreover, there is currently increasing interest in the effect that faceted particles have on the global behavior of granular materials [20, 21]. Angular and faceted shapes are common in geomaterials and very important in civil-engineering applications [22]. In this work we present a systematic theoretical and experimental study of the structural and mechanical properties of deposits of flat faceted particles and discuss the impact that the aspect ratio has on the packing properties of this type of granular media.

The paper is organized as follows: in section 2 the experimental procedure is described in detail; in section 3 we review the theoretical model used in the numerical simulations.

doi:10.1088/1742-5468/2010/06/P06025

J. Stat. Mech. (2010) P06025

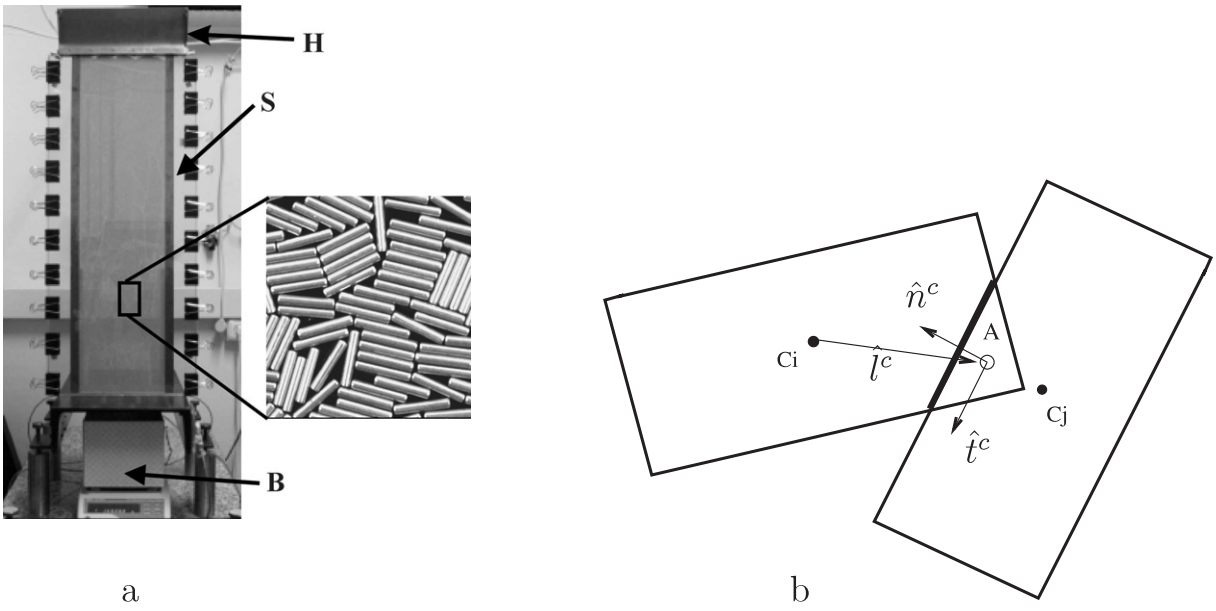

Figure 1. In (a) we show a photograph of the experimental setup. S, two-dimensional silo; H, hopper; B, cardboard box. On the right, there is a zoom of the $d = 5.4$ rods deposited in the bulk of the granular layer. In (b) there is a graphical representation of the contact between two particles. Their interaction is characterized by the overlapping area whose center of mass is at A. The contact branch vector, $\vec{l}_i^c$, joins the center of mass of the particle i and the center of mass of the overlap area. The intersection segment (thick line) identifies the normal, $\hat{n}^c$, and tangential $\hat{t}^c$, directions associated with the contact.

The results of the deposit morphology are reported in section 4 and the details of the micromechanics in section 5. Finally, there is a summary of our conclusions and perspectives.

2. Experiment

The experimental setup consists of a two-dimensional silo of 1.1 mm thickness, 180 mm width and 790 mm height (figure 1). The silo is built with two glass plates separated by two stainless steel strips of 1.1 mm thickness so that the granular material is confined in a monolayer between the plates. The bottom of the silo is flat and formed by two facing metal pieces whose edges touch each other. The particles used in this study are monodisperse stainless steel rods of 1.0 mm diameter and two different lengths (2.4 and 5.4 mm). From now on we will use d, the particle aspect ratio, to characterize the two kinds of rods ($d = 2.4$ and 5.4). It is important to note that the borders of the rods are truncated cones of 0.2 mm length, 1.00 mm long diameter and 0.80 mm short diameter as shown in the zoom of figure 1. More than 5×10^4 and 2×10^4 particles are necessary to fill the silo with $d = 2.4$ and $d = 5.4$ rods respectively.

The granular sample is introduced from the top of the silo through a hopper by pouring the grains along the whole width of the silo in a distributed manner. The feed rate is measured to be around 200 particles per second for the case of 2.4 mm rods and

J. Stat. Mech. (2010) P06025

around 80 particles per second for the case of 5.4 mm rods. Then, after all the particles are deposited, a standard Nikon D40X 10.2 megapixel camera is used to take pictures of the grains inside the silo at two different windows whose width is slightly longer than the width of the silo. The first window covers the region going from the bottom to 110 mm height and the second one covers the region going from 290 to 410 mm height. The images are stored in a computer for further processing and the silo completely emptied by pouring the rods into a cardboard box before a new realization is performed.

Under the proper front illumination the rods reflect an elongated white spot of light, as displayed in the zoom of figure 1. Image processing software is used to identify the position of every rod and its orientation, with a resolution that in most cases was smaller than 0.03 rad. In order to obtain good statistics of the rod orientation and cluster size distributions we performed 100 depositions for each sample, which means that in each window we analyzed more than 7×10^5 and 3×10^5 rods of 2.4 and 5.4 mm length respectively.

3. Model

Since the deposits of experimental rods are quasi-bidimensional, we have performed molecular dynamics simulations of a two-dimensional granular medium composed of identical rectangular particles of aspect ratio d, in units of the shorter side of the particle. The N particles that compose each sample are continuously added at the top of a box with a feed rate of $(714/d)$ particles per second and deposited under the effect of gravity. The box has a width a and height h with lateral and bottom boundaries made of fixed particles to mimic rigid walls. The container width a is always rescaled to the particle aspect ratio $a = 32 \times d$. The simulation runs until the kinetic energy per particle is several orders of magnitude smaller than the initial value, and the stresses no longer vary with time. We have simulated 4000 particles, and the results are averaged over at least fifty different configurations.

We account for particle contact interactions through a recently introduced two-dimensional model, which covers a large variety of grain anisotropies [23]–[25]. In this simplified model, when two particles, i and j, of masses m_i and m_j come into contact they do not deform. Their interaction is simply defined by the contact overlap area and the particles' relative tangential displacement. The vector joining the center of masses of particle i and the overlap area is referred to as the contact branch vector, $\vec{l}_i^{\,c}$ as shown in figure 1(b). The overlap area is characterized by the contact points between the two particles. These two points define a connection line; normal, $\hat{n}^c$, and tangential, $\hat{t}^c$, components of the contact force are defined with respect to this line. Specifically, we consider the normal vector as pointing toward particle i, and the tangent vector as pointing in the same direction as the tangential component of the velocity of particle i, as depicted in figure 1(b). When two vertices overlap with the same side, no special care is necessary as long as the used parameters are always such that the maximum overlap is much smaller than the particle size. In the very unlikely situation where two vertices of one particle overlap with a pair of vertices of a second particle, leading to full face to face interaction, the contact surface is defined by the two middle points between the corresponding closest pairs of vertices. The other steps of the procedure remain the same.

The force associated with contact c acting on particle i is applied at the center of mass of the overlapping area (point A in figure 1(b)), and it is the sum of elastic, $\vec{F}^{e,c}$, and

J. Stat. Mech. (2010) P06025

viscous, $\vec{F}^{\mathrm{v,c}}$, contributions. The total contact force acting on particle i, $\vec{F}_i^{\mathrm{c}} = T^{\mathrm{c}}\hat{t}^{\mathrm{c}} + N^{\mathrm{c}}\hat{n}^{\mathrm{c}}$, decomposes into normal and tangential components. T^{c} satisfies the Coulomb constraint, $T^{\mathrm{c}} = \max(N_s^{\mathrm{c}}, (\vec{F}^{\mathrm{e,c}} + \vec{F}^{\mathrm{v,c}}) \cdot \hat{t}^{\mathrm{c}})$, where the total normal static force, N_s^{c}, is proportional to the total normal force, $N^{\mathrm{c}} = (\vec{F}^{\mathrm{e,c}} + \vec{F}^{\mathrm{v,c}}) \cdot \hat{n}^{\mathrm{c}}$, through the static friction coefficient μ; $N_s^{\mathrm{c}} = \mu N^{\mathrm{c}}$.

The contribution of the elastic force to the total force can be decomposed as

$$\vec{F}^{\mathrm{e,c}} = F_{\mathrm{n}}^{\mathrm{e,c}}\hat{n}^{\mathrm{c}} + F_{\mathrm{t}}^{\mathrm{e,c}}\hat{t}^{\mathrm{c}}, \tag{1}$$

where the normal component of the elastic force is proportional to the overlap area A, divided by a characteristic length L_c of the overlap area, $F_{\mathrm{n}}^{\mathrm{e,c}} = -k_{\mathrm{n}}A/L_c$. The value of L_c is estimated as $1/L_c = 1/(2(1/r_i + 1/r_j))$, where r_i, r_j are the diameters of circles of the same area as particles i and j, respectively [25]. Note that L_c is constant for a monodisperse medium. The tangential elastic force is taken as proportional to the elastic elongation ξ of a contact Cundall–Strack's spring [26], $F_{\mathrm{t}}^{\mathrm{e,c}} = -k_{\mathrm{t}}\xi_c$, where k_{t} is the tangential stiffness. The elastic elongation is zero when the overlap starts and follows the kinematic condition

$$\frac{\mathrm{d}\xi_c(t)}{\mathrm{d}t} = v_{\mathrm{t}}^{\mathrm{c}}, \tag{2}$$

which evolves as long as there is an overlap between the two particles. In the previous expression $v_{\mathrm{t}}^{\mathrm{c}} = (\vec{v}_i^{\mathrm{c}} - \vec{v}_j^{\mathrm{c}}) \cdot \hat{t}^{\mathrm{c}}$ stands for the tangential component of the relative contact velocity of the overlapping pair, while the normal component of the relative velocity follows straightforwardly, $v_{\mathrm{n}}^{\mathrm{c}} = (\vec{v}_i^{\mathrm{c}} - \vec{v}_j^{\mathrm{c}}) \cdot \hat{n}^{\mathrm{c}}$.

The dissipative force at the contact can also be decomposed into normal and tangential viscous force contributions, $F_{\mathrm{n}}^{\mathrm{v,c}} = -m_{\mathrm{r}}\nu_{\mathrm{n}}v_{\mathrm{n}}^{\mathrm{c}}$ and $F_{\mathrm{t}}^{\mathrm{v,c}} = -m_{\mathrm{r}}\nu_{\mathrm{t}}v_{\mathrm{t}}^{\mathrm{c}}$, respectively. Here, $m_{\mathrm{r}} = m_i m_j/(m_i + m_j)$ stands for the pair's reduced mass, while ν_{n} and ν_{t} are the normal and tangential damping coefficients, respectively. The force on particle j associated with contact c follows and ensures overall momentum conservation.

Using the interactions described above, the evolution of the system is given by Newton's equations of motion,

$$m_i\ddot{\vec{r}}_i = \sum_c \vec{F}_i^{\mathrm{c}} - mg\ \hat{e}_y, \tag{3}$$

$$I_i\ddot{\theta}_i = \sum_c (\vec{l}_i^{\mathrm{c}} \times \vec{F}_i^{\mathrm{c}}) \cdot \hat{e}_z, \tag{4}$$

where g represents gravity and I_i stands for the particle moment of inertia. The sums in c run over all the particles in contact with the particle i, and we have assumed that the two-dimensional motion of the grains takes place in a plane normal to $\hat{e}_z$.

The equations of motion, equations (3) and (4), are integrated using a fifth order predictor–corrector algorithm with a numerical error proportional to $(\Delta t)^6$ [27], while the kinematic tangential relative displacement, equation (2), is updated using an Euler algorithm.

In order to model hard particles, the maximum overlap must always be much smaller than the particle size; this is ensured by introducing values for normal and tangential elastic constants, $k_{\mathrm{t}}/k_{\mathrm{n}} = 0.1$ and $k_{\mathrm{n}} = 10^3$ N m^{-1}. The ratio between the normal and tangential damping coefficients is taken as $\nu_{\mathrm{n}}/\nu_{\mathrm{t}} = 3$, while gravity is set to $g = 10$ m s^{-2}.

J. Stat. Mech. (2010) P06025

For these parameters, the time step should be around $\Delta t = 10^{-6}$ s. Although the results we will describe are generic for hard particles, to achieve quantitative comparison with experimental data, we have carried out numerical simulation in which we change both the normal damping coefficient and the static friction coefficient. Thus, we have ensured that the kinetic energy loss and the dynamics of sediment formation are analogous to those seen experimentally. We have converged to $\nu_t = 1 \times 10^3$ s^{-1} and $\mu = 0.6$ as best fit parameters. In all the simulations reported here, we have kept the previous set of parameters and only the particles' aspect ratio has been modified. We have also carried out additional runs (data not shown) using other particles' parameters, and have verified that the trends and properties of the quantities we subsequently analyze are robust to such changes.

4. Morphology of the rod deposits

Figure 2 shows the rod packings obtained numerically for different aspect ratios from $d = 1$ (squares) to $d = 7$. The local mean value of the contact force, normalized by its average value within the whole system, is displayed as a color image on a log-scale. The pictures for squares ($d = 1$) reveal the development of a force network, an intrinsic characteristic of granular solids. Moreover, the interparticle force distribution decays exponentially [17]. In contrast, for elongated rods the force is transmitted much more homogeneously, leading to a visible increase on the force with the deposit depth. Force transmission is characterized in this case by a Gaussian distribution [17].

In order to characterize the packing morphology, we first examine the orientations of the particles both numerically and experimentally. The distributions of particle orientation $f(\theta)$ with respect to the horizontal are illustrated in a polar plot in figure 3 for $d = 1$, 2.4 and 5.4. The agreement between the experimental and numerical results demonstrates the predictive accuracy of our numerical simulation scheme. It can clearly be seen that long particles most probably lie parallel to the substrate ($\theta = 0$ and π), while the most unlikely position corresponds to standing rods ($\theta = \pi/2$). This result is in excellent agreement with previous observations of rod packings [28]. Experimentally, for elongated particles the fraction of horizontally aligned particles is larger than in computer simulations. We believe that in experiments, the slightly round end of the steel rods prevents vertical alignment and favors particle rotation toward a horizontal orientation. In simulations, the strict angular shape results in an increase in the number of vertically oriented particles. As the aspect ratio decreases, there is a shift in the most probable orientation, leading to a peaked distribution at an intermediate orientation. For squares, the most probable orientation turns out to be $\theta = \pi/4$, i.e. the squares have one of their diagonals parallel to gravity. In all cases the orientation distribution displays an expected symmetry with respect to $\theta = \pi/2$, i.e. the direction of gravity. To obtain the particle orientation distributions we have disregarded the contribution of particles located close to the system walls, along which rods display a strong preferential alignment. The effect of the walls, which can be significant in stress transmission, as reported previously in the case of discs [29], needs to be systematically studied in a future work.

The packing morphology has also been examined through the particle radial distribution function, which can be expressed as:

$$g(r) = \left\langle \frac{N(r + \delta r)}{2\pi r \delta r \rho} \right\rangle, \tag{5}$$

J. Stat. Mech. (2010) P06025

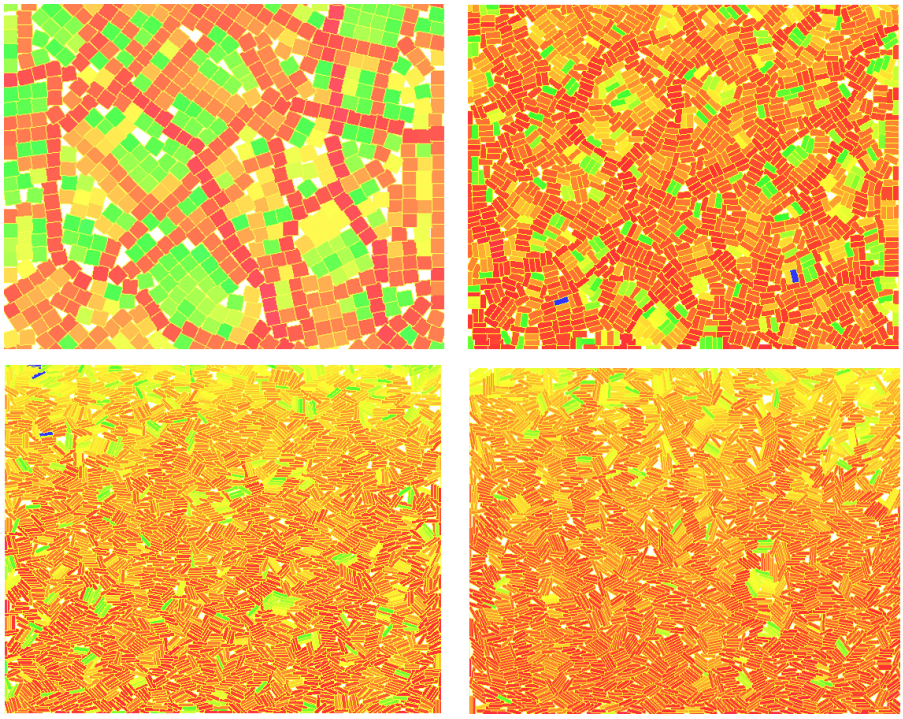

Figure 2. Packings of particles obtained for different aspect ratios, numerical graphs for $d = 1, 2.4, 5.4$ and 7. The color map displays on a log-scale the local mean value of the contact forces on each particle, normalized by the average value within the whole system.

where $\rho = N_T/S$ is the average number of rods per unit of area in the whole packing and is measured by counting the total number of rods N_T whose center of mass lies in the analyzed area. $N(r + \delta r)$ accounts for the number of particles with their center of mass at a distance r within a differential area $\delta S = 2\pi r \delta r$. In figure 4(a) and (b), the radial distribution function, $g(r)$, is illustrated for the experimental and the numerical deposition of particles with $d = 2.4$ and 5.4. In both cases the first result that becomes apparent is the existence of peaks at $r = 1, 2, 3, \ldots$, which correspond to structures where $2, 3, 4, \ldots$ rods are perfectly aligned with their long faces parallel each other (labeled as LL in the graphs). Additionally, other peaks are present at $r = 1.7, 2.7, \ldots$ for $d = 2.4$, and at $r = 3.2, 4.2, \ldots$ for $d = 5.4$. These correspond to rod structures where a long face is aligned with a short face and are labeled as LS in the figures. Finally, we also observe two local maximums in $r = 2.4$ and 5.4 for $d = 2.4$ and 5.4 respectively. These peaks correspond to rods aligned by their short faces and are labeled in the graphs by SS.

In order to gain further insight into the local structure of rod alignment, we have measured the radial orientational function $Q(r)$, defined as

$$Q(r) = \langle \cos\left(2(\theta_i - \theta_j)\right)\delta(\mathbf{r}_{ij} - r)\rangle \tag{6}$$

where θ_i and θ_j are the angular orientations of particles i and j, respectively.

This distribution function provides additional quantitative information on the local structure of the rod packings because configurations where the two rods are perpendicular to each other (LS configurations in figure 4) contribute -1 to $Q(r)$, while rods aligned

J. Stat. Mech. (2010) P06025

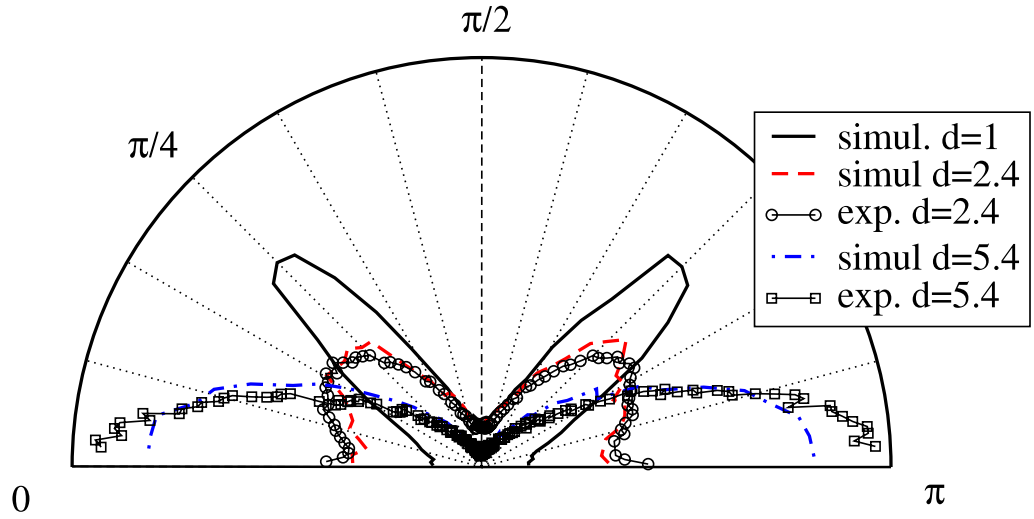

Figure 3. Polar orientation distributions of particles for several aspect ratios. Experimental and numerical results are shown for comparison.

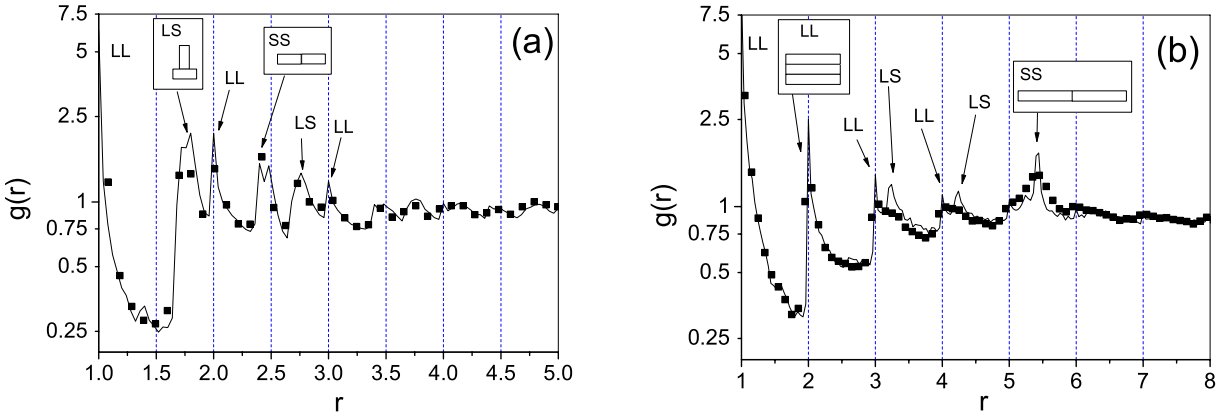

Figure 4. Radial distribution functions obtained experimentally (■) and in numerical simulations (continuous line) for rod deposits with different aspect ratios, d. (a) $d = 2.4$ and (b) $d = 5.4$.

along their long faces (LL configurations) or along their short faces (SS configurations) contribute 1. Experimental and numerical data for $d = 2.4$ (figure 5(a)) and $d = 5.4$ (figure 5(b)) are shown for comparison. As expected, all the configurations observed in figure 4 are also recovered by $Q(r)$, which displays maximum peaks for LL and SS configurations and minimum peaks for LS configurations. Furthermore, the $Q(r)$ signals the presence of additional structures, like LS at $r = 5.2$ for $d = 5.4$, which are harder to identify from the radial distribution function. The results of $Q(r)$ for $d = 5.4$ display higher values for experiments than for simulations, especially for high r. This result is consistent with the increased tendency of experimental rods to align horizontally (figure 3) which has been attributed to the differences between experimental and simulated rod shapes. $Q(r)$ should decay to zero for long distances if the angular correlations are short range. In this case, the nonvanishing asymptotic value observed is a

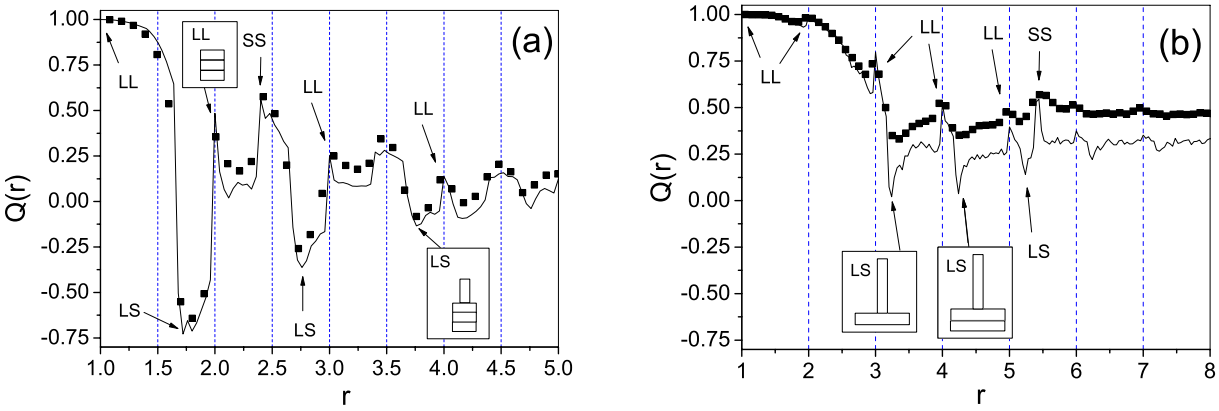

Figure 5. Radial orientation distribution functions, $Q(r)$, as defined in equation (6), obtained experimentally (■) and in numerical simulations (continuous line) for rod deposits with different aspect ratios, d. (a) $d = 2.4$ and (b) $d = 5.4$.

Table 1. Average values of the packing fraction (ϕ) and the mean coordination number (Z) for different aspect ratios. The experimental values of Z are not displayed as their measurement is not possible.

	$d = 1$ (num)	$d = 2.4$ (num)	$d = 2.4$ (exp)	$d = 5.4$ (num)	$d = 5.4$ (exp)	$d = 7$ (num)
ϕ	0.882	0.855	0.979	0.807	0.896	0.786
Z	3.32	3.40	—	3.50	—	3.45

consequence of the preferred rod orientation along the whole area of the packing which is a tendency particularly marked in the experiments. The combined analysis of the radial distribution function, $g(r)$, and the angular correlation, $Q(r)$, has clarified the structure of these packings, the marked tendency of rods to align parallel to the substrate and the development of long-ranged angular correlations.

Table 1 shows how the packing fraction changes with particle elongation. We observe a monotonous decrease as the particle becomes more anisotropic. However, we cannot exclude an initial increase for slightly deformed squares; it is known that in ellipsoids [12] the packing fraction exhibits a maximum for aspect ratios of around 3/2. For all aspect ratios the deposits are highly compacted; so we have also analyzed the cluster (or domain) size distributions of aligned particles. Two rods are regarded as part of the same cluster if there is any contact between them and any of their flat faces have the same orientation, independently of whether the alignment is SS, LL or LS [17]. Experimentally, two rods belong to the same cluster if the distance between any point of their surfaces is smaller than 0.1 mm and the relative orientation between any of their faces is smaller than 0.05 rad. In practice, particle orientation is defined by a vector parallel to the largest side of the rod and both relatively perpendicular, and parallel orientations are admitted. In the simulations, we use the same angular criterion and consider that two particles are in contact when the modulus of the interparticle force is larger than 10^{-6} times the average contact force.

In figure 6(a) both experimental and numerical results for the cluster size distributions $D(s)$ are shown on a log–log scale. The graph indicates a remarkable agreement between

J. Stat. Mech. (2010) P06025

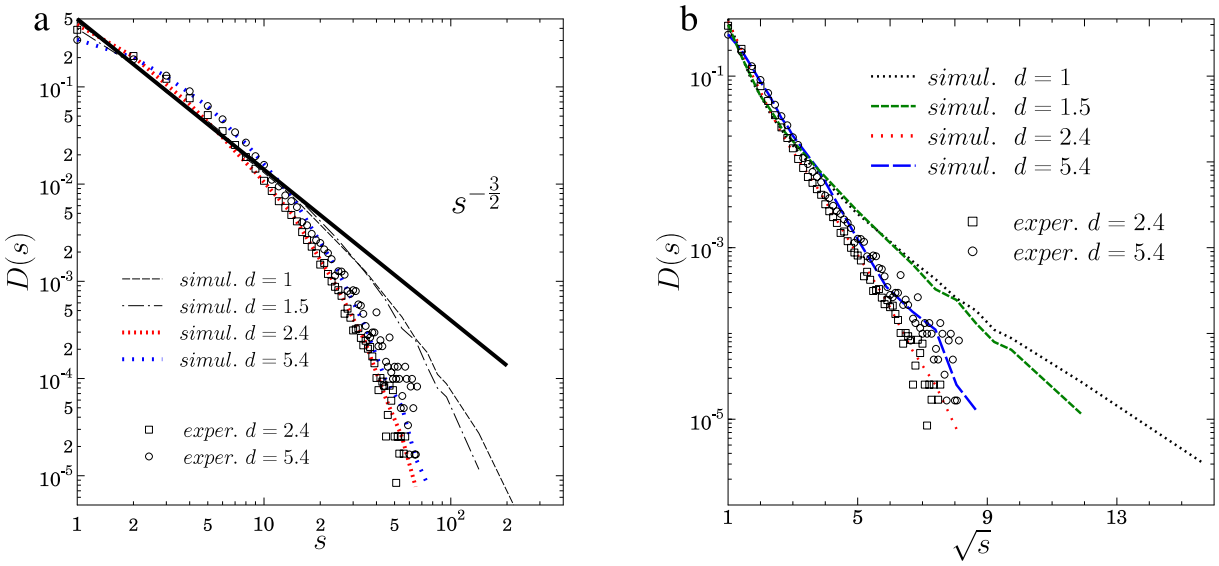

Figure 6. Cluster size distribution, $D(s)$, of particle deposits with different aspect ratios. (a) $D(s)$ on a log–log scale to display the algebraic decay at small and intermediate cluster sizes; (b) linear-log scale of $D(s)$ as a function of $\sqrt{s}$.

experimental and simulation results for the two aspect ratios shown, $d = 2.4$ and 5.4. We also present numerical results corresponding to a systematic study of the cluster size distribution for different aspect ratios. For squares, $d = 1$, the cluster size distribution follows the power law $D(s) \sim s^{-3/2}$ with an exponential cutoff. This result was explained in [17] in the context of aggregation systems with injection [30] or random multiplicative processes [31]. Indeed $D(s) \sim s^{-3/2}$ can be understood as the orientational version of the critical q-model proposed for describing force propagation in a granular packing [32, 33]. Very recently, a similar result was obtained for a two-dimensional ensemble of birefringent discs, where the force network was described by a simple graph [33]. Figure 6(a) displays a faster decay of the big cluster size distribution. This behavior is evidence of the structural differences between big and small clusters, rather than a finite size effect, as shown in [17]. Consistent with this picture, long force chains isolate compact clusters which contain, on average, a larger number of particles than the force chains themselves. Therefore, the power law decay of the cluster size distribution can be attributed to force chains and the asymptotic faster decay to compact clusters.

The semi-log graph of figure 6(b) displays the distribution of clusters of aligned particles in terms of $\sqrt{s}$. As the grains elongate, the asymptotic decay of the cluster distribution gradually deviates from the algebraic decay. This is a consequence of the fact that the orientation of the particles, forming a $\pi/4$ angle, becomes less favored. Hence, for very elongated particles the algebraic decay disappears and the exponential decay in terms of $\sqrt{s}$ becomes dominant. This asymptotic, exponential decay can be understood in the framework of percolation theory. Due to the high compaction fraction of the particle deposits (see table 1), the compact structure formed by aligned particles is far above the percolation threshold in a 2D square lattice ($p_c = 0.5$). For such compact clusters it is known [34] that, above the percolation threshold, the first correction to the critical cluster size distribution obeys $D(s) \sim \mathrm{e}^{-\sqrt{s}}$.

J. Stat. Mech. (2010) P06025

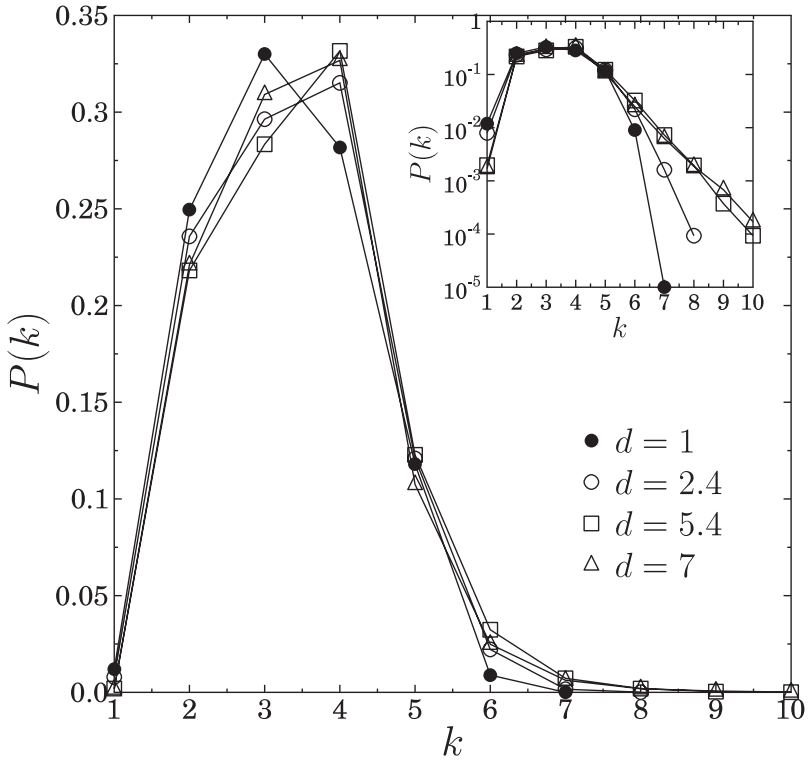

Figure 7. Coordination number distribution, obtained for deposits of particles with different aspect ratios.

Cluster analysis has shown the impact of the particle aspect ratio on the internal packing structure. To clarify how forces propagate in these deposits, we will consider in more detail the micromechanical properties of rod packings in the following section.

5. Micromechanics

Force transmission in granular media occurs only through particle contacts. Therefore, the distribution of the number of contacts, k, has an important influence on force propagation within deposits. Figure 7 displays the contact number distributions, $P(k)$, obtained numerically for particle deposits with different aspect ratios. Clearly, squares are the only particles that show a maximum probability at $k = 3$. Their narrow distribution (see inset of figure 7) also denotes the presence of well defined force chains, in agreement with the cluster structure discussed in the previous section. For elongated particles the peak is shifted to $k = 4$ and the probability decays less abruptly than for squares (see inset of figure 7). This means that the longer the rod, the higher the mean number of contacts per particle (Z), as shown in table 1. Moreover, it indicates a trend towards the formation of bulk type clusters, suggesting a vertical force transmission. This result is in good agreement with previous experiments and simulations in the 3D packing of rods [11, 18]. Additionally, the existence of arcs, which is indicated by the presence of particles with two contacts, also decreases with an increasing particle aspect ratio.

The contact network of granular materials can be conveniently characterized in terms of the contact fabric tensor, $F_{\alpha\beta}$. This magnitude measures the average contact number

J. Stat. Mech. (2010) P06025

density for a given direction in the assembly. It may be used, therefore, to examine whether the packing is isotropic or there is directional ordering [35, 36]. Thus, the contact fabric tensor, $F^i_{\alpha\beta}$, of a single particle i is defined as

$$F^i_{\alpha\beta} = \sum_{c=1}^{C_i} l^c_{i,\alpha} l^c_{i,\beta} \tag{7}$$

where the dyadic product of the normalized branch vectors associated with particle i at contact c, $\vec{l}^c_i$, is summed over all particle contacts, C_i. The mean fabric tensor, $\bar{F}_{\alpha\beta}$, can then be expressed as

$$\bar{F}_{\alpha\beta} = \left\langle \sum_{i=1}^{N} w_v F^i_{\alpha\beta} \right\rangle \tag{8}$$

where w_v is its average weight. For simplicity's sake we choose the simplest weighting, and use particle-center averaging, where $w_v = 1$ if the center of the particle lies inside the averaging area and $w_v = 0$ otherwise [35, 36]. For systems composed of monodisperse particles, the tensor $\bar{F}_{\alpha\beta}$ is normalized so that its trace, $\mathrm{Tr}(\bar{F}) = Z$, reduces to the mean coordination number Z. As a result, the deviator of the fabric tensor, i.e. $\bar{F}^d_{\alpha\beta} = \bar{F}_{\alpha\beta} - \mathrm{Tr}(F)I$, is a measure of the anisotropy of the contact network [35, 36].

In figure 8, the polar contact distributions for squares ($d = 1$) and elongated particles ($d = 5.4$) are shown for comparison. We also show the principal directions of the mean fabric tensor, $\bar{F}_{\alpha\beta}$, which validates the consistency of the numerical data. The tendency of elongated particles to align horizontally is manifested by a large anisotropy in the effective number of contacts. Elongated particles, lying horizontally, generate contacts more easily with particles above and below at angles close to $\theta = 0$ and π. Squares, in contrast, align their diagonals parallel with and perpendicular to gravity, and the contact probability is bidirectional. The distribution of branch vectors, therefore, provides an alternative and, consistent, procedure for analyzing the structure of particle packings.

We can correlate this microstructure with stress transmission by studying the micromechanical properties of the granular pile. To this end, we introduce the stress tensor of a single particle,

$$\sigma^i_{\alpha\beta} = \sum_{c=1}^{C_i} l^c_{i,\alpha} F^c_{i,\beta}, \tag{9}$$

which is defined in terms of the total contact force $\vec{F}^c_i$ that particle i experiences at contact c, as derived in section 3. In equation (9), $\vec{l}^c_i$ is the branch vector related to the contact c, and the sum runs over all the contacts C_i of particle i. Making use of the particle-center averaging introduced in equation (8) the mean stress reads

$$\bar{\sigma}_{\alpha\beta} = \sum_{i=1}^{N} w_v \sigma^i_{\alpha\beta} \tag{10}$$

where the sum runs over the whole system.

In figure 9, the distribution of the principal stress directions for all the single particles in the sample is shown for $d = 1$ and 5.4 in polar coordinates. In each plot,

J. Stat. Mech. (2010) P06025

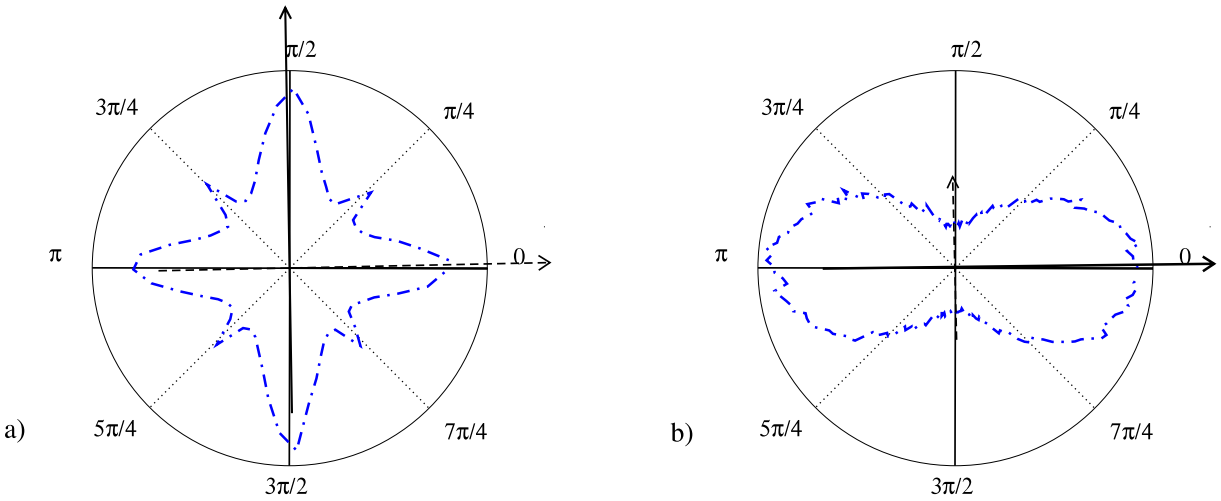

Figure 8. Polar distribution of the branch vectors for (a) squares and (b) elongated particles with aspect ratio $d = 5.4$. The continuous (discontinuous) arrow represents the largest (smallest) eigenvalue of the mean fabric tensor.

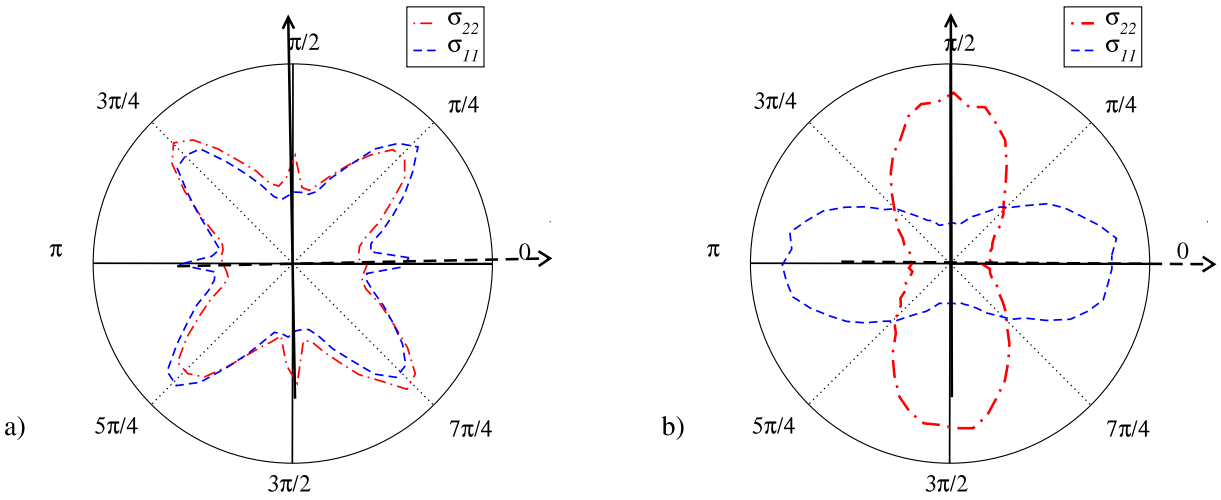

Figure 9. Polar distribution of the principal directions of the *local stress* for deposits of (a) squares and (b) elongated particles with aspect ratio $d = 5.4$. The continuous (discontinuous) arrow represents the largest (smallest) eigenvalue of the mean stress tensor.

the continuous arrow corresponds to the largest eigenvalue of the mean stress tensor, while the discontinuous line denotes the smallest. For squares, force distributions, as shown in figure 9(a), display a clear symmetry and are evidence that forces are mainly transmitted along the $\pi/4$ and $3\pi/4$ directions. As we note below, this has a marked impact on the stress distribution within the sample. For elongated particles, however, figure 9(b) indicates that forces are preferentially transmitted parallel to gravity. Thus, stress transmission in deposits of elongated particles displays a high degree of alignment with the external gravity field. Note that for these rods the eigenvalues of the stress

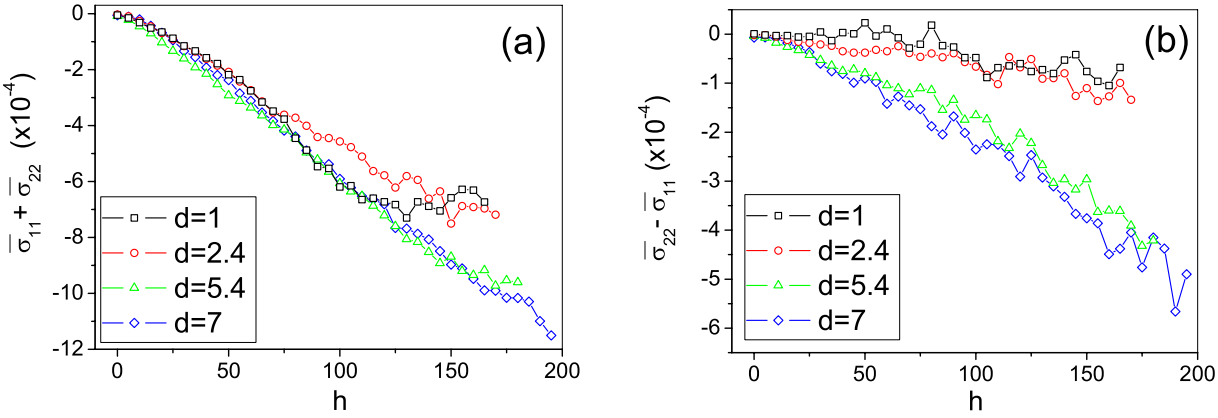

Figure 10. Profiles of the trace (a) and deviator (b) of the mean stress tensor. Results for several aspect ratios are shown. In all cases the stress is rescaled by the normal stiffness, k_n, and the height h is expressed in units of the particle shortest side.

tensor are perpendicular to those of the fabric tensor displayed in figure 8. Therefore, the structural analysis of local contacts provides a stronger indication of the mechanical properties of a deposit. Recent results for irregular particles [37] have shown that the orientation of elongated particles is strongly associated with the stability of the packing, and that forces are mainly transmitted through contacts parallel to the shortest particle dimension. Stress transmission is consistent with this picture, but it also indicates that for more isotropic particles stress transmission changes its nature. The peculiar orientation of squares leads to a bidirectional contact ordering, and stress transmission forming an angle of 45° with gravity. Hence, we see how the changes in microstructure induced by particle geometry determine stress transmission and localization in particle deposits.

The previous results correspond to global averages, but we have also analyzed spatial stress distribution within the packing. Specifically, figures 10 and 11 display the trace, deviator and eigenvalues ($\bar{\sigma}_{11}$ and $\bar{\sigma}_{22}$) of the mean stress tensor, $\bar{\sigma}_{\alpha\beta}$, as a function of the deposit depth h, for particle deposits with different aspect ratios. In all the cases analyzed, the two eigenvectors are very closely parallel to the Cartesian axis; the largest eigenvalue corresponds to a direction which closely follows the direction of gravity. In order to obtain the mean stress as a function of the distance from the packing surface, we use equation (10), and restrict the sum to all particles whose centers lie in a layer of sector ($h - \Delta h < h < h + \Delta h$), where Δh is five times the length of the shorter side of the particle.

The nature of the stress transmission reflects on the two eigenvalues ($\bar{\sigma}_{11}$ and $\bar{\sigma}_{22}$) as well as the trace and the deviator. Figure 10(a) reveals that, for rods which are not very elongated, the trace of the stress tensor saturates with increasing depth. This result is in good agreement with the scenario proposed for squares depositions, which is compatible with a heterogeneous force transmission characterized by the development of well defined force chains and an exponential distribution of the interparticle normal forces [17]. Then, as the force is mainly transmitted in the $\pi/4$ and $3\pi/4$ directions, there are force chains directed towards the walls which screen the apparent weight at the bottom of the granular column and lead to total pressure saturation in the silo. Further evidence of this behavior

J. Stat. Mech. (2010) P06025

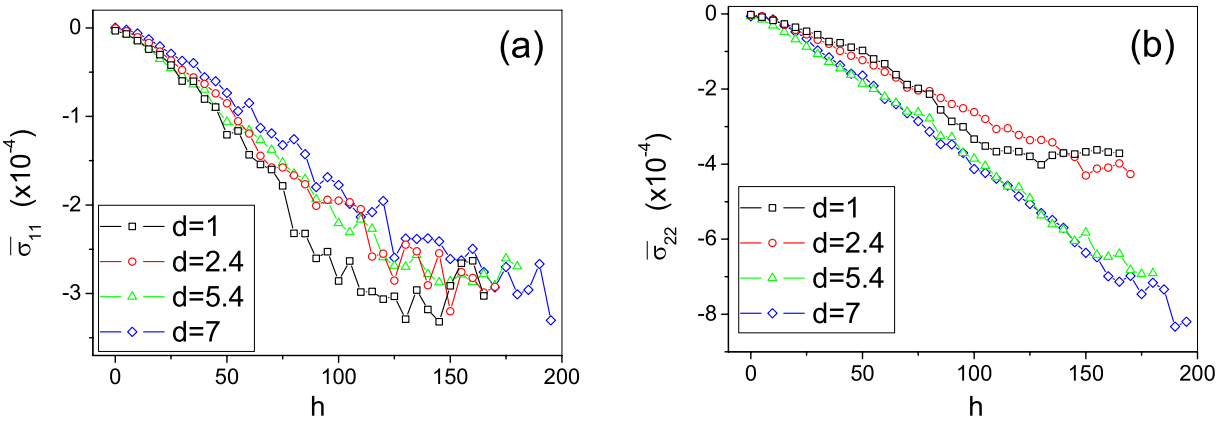

Figure 11. Profiles of the eigenvalues of the mean stress tensor, (a) σ_{11} and (b) σ_{22}. Results for several aspect ratios are shown. In all cases the stress is rescaled by the normal stiffness, k_n, and the height h is expressed in units of the particle shortest side.

is the fact that for squares, the two eigenvalues of the mean stress tensor are roughly similar to each other (see figure 11(a) and (b)).

For elongated particles, stress transmission is dominated by the contribution parallel to gravity ($\bar{\sigma}_{22}$) whose values are much higher than the stress in the horizontal direction ($\bar{\sigma}_{11}$). This asymmetry in the stress transmission is quantified through the depth-dependent deviator of the mean stress, as displayed in figure 10(b). Moreover, for elongated rods, the behavior of the trace (figure 10(a)) and the stress eigenvalues (figure 11(a) and (b)) clearly suggest that the saturation of the stress with the deposit depth is strongly inhibited. In particular, it is remarkable that $\bar{\sigma}_{22}$ grows linearly with increasing depth without displaying pressure saturation. This result is a consequence of the horizontal alignment of the flat faces of the rods, which causes anisotropic force transmission from top to bottom. Although we cannot discard eventual saturation for sufficiently deep deposits, the outcomes clearly indicate that the strong tendency of the particles to align horizontally favors stress transmission parallel to gravity, which destroys stress localization along force chains.

6. Conclusions

In this work we present experimental and numerical results of the topological and mechanical properties displayed by bidimensional deposits of faceted particles with different aspect ratios. In all cases the topology is dominated by the formation of ordered structures of aligned rods. We believe that the origin of this high ordering lies in the fact that the particles are poured in a quasi-sequential procedure. Hence, during deposition the particles are allowed to explore different configurations and relax to the one that minimizes the energy. Elongated particles tend to align horizontally. Then the stress is mainly transmitted from top to bottom, which is revealed by the asymmetric distribution of the local stress. Consequently the trace of the stress tensor does not present saturation with the depth, and the deviator of the mean stress tensor increases continuously with

the height of the column. When the particles become more symmetric, their orientation deviates from the horizontal and, for the limiting case of squares, becomes oriented with a diagonal parallel to gravity. This causes a symmetrical transmission of the local stress at angles $\pi/4$ and $3\pi/4$ with respect to the direction of gravity. As a result, the trace of the mean stress tensor saturates for a given depth in the layer, as is expected for granular materials composed of spherical particles. We can also conclude that stress localization is highly correlated to pressure saturation and the appearance of Jansen's effect. The strong dominance of the vertical component of the stress for elongated rods indicates that if saturation develops for deeper deposits, such a saturation will be qualitatively different from the one observed for isotropic grains. It is worth noting that we have focused on intrinsic stress saturation because the results discussed correspond to silos where the lateral walls are smooth. Wall-induced irregularities provide an additional mechanism for stress saturation; the interplay between particle anisotropy and wall roughness will be addressed elsewhere.

Acknowledgments

The Spanish MICINN (Projects FIS2008-06034-C02-01, FIS2008-06034-C02-02 and FIS2008-04386) and the University of Navarra (PIUNA Program) have supported this work. RCH also acknowledges the financial support of the Spanish MICINN, through a *Ramón y Cajal Program*.

References

[1] Garcia-Rojo R, Herrmann H J and McNamara S (ed), 2005 *Powders and Grains* (Rotterdam: Balkema)
[2] Jaeger H M, Nagel S R and Behringer R P, 1996 *Rev. Mod. Phys.* **68** 1259
[3] Aranson I S and Tsimringy L S, 2006 *Rev. Mod. Phys.* **78** 641
[4] Pöschel T and Schwager T, 2005 *Computational Granular Dynamics* (Berlin: Springer)
[5] Liu C, Nagel S R, Schecter D A, Coppersmith S N, Majumdar S, Narayan O and Witten J P, 1995 *Science* **269** 513
Meuth D M, Jaeger H M and Nagel S R, 1998 *Phys. Rev.* E **57** 3164
[6] Majmudar T S and Behringer R P, 2005 *Nature* **435** 1079
[7] Meuth D M, Jaeger H M and Nagel S R, 1998 *Phys. Rev.* E **57** 3164
[8] Lovoll G, Maloy K J and Flekkoy E G, 1999 *Phys. Rev.* E **60** 5872
[9] Tsoungui O, Vallet D and Charmet J, 1998 *Granular Matter* **1** 65
[10] Gallas J A C and Sokolowski S, 1993 *Int. J. Mod. Phys.* B **7** 2037
[11] Villarruel F X, Lauderdale B E, Mueth D M and Jaeger H M, 2000 *Phys. Rev.* E **61** 6914
Lumay G and Vandewalle N, 2004 *Phys. Rev.* E **70** 051314
Lumay G and Vandewalle N, 2006 *Phys. Rev.* E **74** 021301
[12] Donev A, Cisse I, Sachs D, Variano E A, Stillinger F H, Connelly R, Torquato S and Chaikin P M, 2004 *Science* **303** 990
[13] Nielsen J, 1998 *Phil. Trans. R. Soc.* A **356** 2667
Zhong Z, Ooi J Y and Rotter J M, 2001 *Eng. Struct.* **23** 756
[14] Blouwolff J and Fraden S, 2006 *Europhys. Lett.* **76** 1095
[15] Desmond K and Franklin S V, 2006 *Phys. Rev.* E **73** 031306
[16] Zuriguel I, Mullin T and Rotter J M, 2007 *Phys. Rev. Lett.* **98** 028001
Zuriguel I and Mullin T, 2008 *Proc. R. Soc.* A **464** 99
[17] Hidalgo R C, Zuriguel I, Maza D and Pagonabarraga I, 2009 *Phys. Rev. Lett.* **103** 118001
[18] Wouterse A, Luding S and Philipse A P, 2009 *Granular Matter* **11** 169
[19] Guises R, Xiang J, Latham J and Munjiza A, 2009 *Granular Matter* **11** 281
[20] Azéma E, Radjai F, Peyroux R and Saussine G, 2007 *Phys. Rev.* E **76** 011301
[21] Azéma E, Radjai F and Saussine G, 2009 *Mech. Mater.* **41** 729
[22] Nouguier-Lehon C, Cambou B and Vincens E, 2003 *Int. J. Numer. Anal. Meth. Geomech.* **27** 1207
[23] Alonso-Marroquín F and Herrmann H J, 2004 *Phys. Rev. Lett.* **92** 054301

J. Stat. Mech. (2010) P06025

Wittel F *et al*, 2004 *Phys. Rev. Lett.* **93** 035504
[24] Tillemans H J and Herrmann H J, 1995 *Physica* A **217** 261
Kun F and Herrmann H J, 1999 *Phys. Rev.* E **59** 2623
[25] Kun F and Herrmann H J, 1996 *Int. J. Mod. Phys.* C **7** 837
[26] Cundall P A and Strack O D L, 1979 *Géotechnique* **29** 47
[27] Allen M P and Tildesley D J, 2003 *Computer Simulation of Liquids* (Oxford: Oxford University Press)
[28] Stokely K, Diacou A and Franklin S V, 2003 *Phys. Rev.* E **67** 051302
[29] Bartos I and Janosi I M, 2007 *Granular Matter* **9** 81
Zuriguel I, Mullin T and Arevalo A, 2008 *Phys. Rev.* E **77** 061307
[30] Takayasu H, Nishikawa I and Tasaki H, 1988 *Phys. Rev.* A **37** 3110
Huber G, 1991 *Physica* A **170** 463
[31] Moukarzel C F, 2002 *J. Phys.: Condens. Matter* **14** 2379
[32] Coppersmith S N, Liu C, Majumdar S, Narayan O and Witten T A, 1996 *Phys. Rev.* E **53** 4673
[33] Wambaugh J F, 2006 arXiv:cond-mat/0603314
[34] Stauffer D and Aharony A, 1991 *Introduction to Percolation Theory* (London: Taylor and Francis)
[35] Lätzel M, Luding S and Herrmann H J, 2000 *Granular Matter* **2** 123
[36] Madadi M, Tsoungui O, Lätzel M and Luding S, 2004 *Int. J. Solids Struct.* **41** 2563
[37] Peña A, García-Rojo R and Herrmann H J, 2007 *Granular Matter* **9** 279

J. Stat. Mech. (2010) P06025